PHOTONIC SENSORS / Vol. 6, No. 1, 2016: 1–25

Invited Paper

Research Progress in the Key Device and Technology for Fiber Optic Sensor Network

Deming LIU, Qizhen SUN*, Ping LU, Li XIA, and Chaotan SIMA

School of Optical and Electronic Information, Huazhong University of Science and Technology; National Engineering Laboratory for Next Generation Internet Access System, Wuhan, 430074, China

*Corresponding author: Qizhen SUN E-mail: qzsun@hust.edu.cn

Abstract: The recent research progress in the key device and technology of the fiber optic sensor network (FOSN) is introduced in this paper. An architecture of the sensor optical passive network (SPON), by employing hybrid wavelength division multiplexing/time division multiplexing (WDM/TDM) techniques similar to the fiber communication passive optical network (PON), is proposed. The network topology scheme of a hybrid TDM/WDM/FDM (frequency division multiplexing) three-dimension fiber optic sensing system for achieving ultra-large capacity, long distance, and high resolution sensing performance is performed and analyzed. As the most important device of the FOSN, several kinds of light source are developed, including the wideband multi-wavelength fiber laser operating at C band, switchable and tunable 2 μm multi-wavelength fiber lasers, ultra-fast mode-locked fiber laser, as well as the optical wideband chaos source, which have very good application prospects in the FOSN. Meanwhile, intelligent management techniques for the FOSN including wideband spectrum demodulation of the sensing signals and real-time fault monitoring of fiber links are presented. Moreover, several typical applications of the FOSN are also discussed, such as the fiber optic gas sensing network, fiber optic acoustic sensing network, and strain/dynamic strain sensing network.

Keywords: Fiber optic sensor network; fiber optic sensor laser; intelligent management; fiber optic gas sensing; fiber optic acoustic sensing; fiber optics strain sensing

Citation: Deming LIU, Qizhen SUN, Ping LU, Li XIA, and Chaotan SIMA, "Research Progress in the Key Device and Technology for Fiber Optic Sensor Network," *Photonic Sensors*, 2016, 6(1): 1–25.

1. Introduction

Due to the distinct advantages of light weight, small size, high sensitivity, immunity to electromagnetic interference, and ease to network, fiber optic sensors have been intensively studied for measuring numerous parameters including temperature, strain, refractive index, vibration, displacement, etc. in the past 40 years. Along with the bloom of optical fiber sensors and the tidal wave of Internet of Things (IOT), the fiber optic sensing network is becoming an inevitable tendency for the sensing industry [1]. Especially for the application areas requiring multipoint and large area measurement, such as structural health monitoring and geophysical surveying, the fiber optic sensing networks are ideal solutions. For a typical fiber optic sensing network, the fiber sensors can be

Received: 15 November 2015 / Revised: 6 December 2015

DOI: 10.1007/s13320-015-0299-z
Article type: Review

multiplexed by specific schemes, including time division multiplexing (TDM), wavelength division multiplexing (WDM), frequency division multiplexing (FDM), coherent division multiplexing (CDM), and space division multiplexing (SDM) [2−6]. Recently, following the development trend of the large capacity, long distance, and high resolution of the fiber optic sensing network, the hybrid of above multiplexing schemes are intensively studied. By exploring high-performance light sources and demodulation modules, the information of each sensor unit can be interrogated, enabling the corresponding sensing parameters to be detected.

Stable and compact light sources, with wide bandwidth, multiple and selective operating wavelengths, ultra-short pulse width, high output power, or other special properties, are essential for the fiber optic sensing network to support specific multiplexing schemes. As a promising candidate of specialized light sources, fiber lasers have attracted considerable attention due to their overwhelming advantages of compatibility toward fiber, flexibility in wavelength control, high beam quality, low pump-power requirements, and reliability in harsh environment [7].

In addition, the intelligent management especially the survivability of the fiber optic sensor network, is also important. For example, the fiber optic sensor networks usually work in harsh environment with large temperature difference, high pressure, strong magnetic field, etc. Thus, the fiber fracture could happen occasionally [8], while it may cost much time and manpower to locate the fiber breakpoint in the sensor network with the large coverage area and complex structure [9]. Therefore, automatic and precision fiber fault locating techniques should be developed.

In this paper, we review the efforts to advance the fields of fiber optic sensing networks. (1) Firstly, a brief description of various multiplexing schemes provides some insight into the advantages and remaining challenges of them. Then, we expect to build up a highly adaptive fiber optic sensor network (FOSN) with large capacity and multi-parameters/functions/mechanisms integration, by employing hybrid WDM/TDM multiplexing techniques and matrix topology architecture similar to the fiber communication passive optical network (PON). Consequently, on account of a selected hybrid TDM/WDM/FDM scheme, a novel sensing network with linear typology along a single fiber is established, mainly focusing on ultra-large capacity, long distance, and high resolution sensing performance. (2) Secondly, as the most important device of the FOSN, several kinds of fiber laser, including the wideband multi-wavelength fiber laser operating at C band, switchable and tunable 2 μm multi-wavelength fiber lasers, ultra-fast mode-locked fiber laser, and optical wideband chaos source, are explored to meet the requirements of the FOSN. (3) Thirdly, intelligent management techniques of the FOSN, including the wide bandwidth, high resolution, and high speed optical spectrum demodulation, as well as the real-time and precisely fault monitoring of fiber link are performed. (4) Finally, several typical applications of the FOSN are discussed, including the fiber optic gas sensing network, fiber optic acoustic sensing network, and quasi-distributed static/dynamic strain sensing network.

2. Networking technology of the fiber optic sensors

Accompanied by the development of fiber optic communication technologies, fiber optic sensing technologies are greatly improved. At present, the reported FOSN techniques are mainly focused on the various sensor multiplexing schemes, including WDM, TDM, SDM, FDM, and CDM, or the combinations of them.

2.1 Single division multiplexing schemes

TDM is the simplest and earliest reported multiplexing scheme, in which the fiber sensors in

the sensing link are usually arranged by the cascaded way with a delay line inserted between two adjacent fiber sensors to separate them in time domain. Differed by the time delay to receive the sensing signal, different fiber sensors can be distinguished and located. Many researchers have been focused on increasing the capacity and the spatial resolution of the TDM scheme. For instance, the capacity of the fiber Bragg grating (FBG) based TDM scheme has increased from tens to hundreds points in the past decades [10−12]. Recently, Q. Z. Sun and C. Y. Hu separately reported the TDM technique based on ultra-weak FBGs and demonstrated an FOSN along a single fiber with over 1000 sensors [13, 14]. However, limited by the topological structure and time slot based locating method, the spatial resolution of the TDM scheme is still limited.

The WDM scheme has been very mature in the wavelength encoded fiber sensors. Optical fiber sensors always occupy a particular bandwidth of the light spectrum. By using a broadband light source and allocating different bandwidths to the fiber sensors, different fiber sensors can be distinguished through the wavelengths of sensing signals. For the FBG sensor network, the capacity of the WDM sensing network is usually limited to only several dozen, decided by the wavelength range of the light source and bandwidth allocated to each FBG [15, 16].

The most important and typical technique of FDM is the frequency modulation continuous wave technique (FMCW), which is also called the optical frequency domain reflector (OFDR). By employing the narrow linewidth light source and high speed acquisition setup, the OFDR can realize a very high spatial resolution and large capacity. Kazumasa Takada reported a high spatial resolution of 850 μm with a fiber optic frequency encoder in 1992 [17]. Brooks A. Chiders achieved a test with 3000 FBGs distributed on four 8-meter fibers. However, the system cost is relatively high, and the application in the long-distance detection is limited [18].

The CDM technology multiplexes the interferometric fiber sensors like the Mach-Zehnder interferometer, Michelson interferometer, and the Fabry-Perot (FP) interferometer. This technique was first proposed by Brooks in 1985 [19]. However, it requires a compensating interferometer for each sensor to realize demodulation, which cannot satisfy the requirement for large capacity applications.

Besides, sensors on different fibers can be multiplexed through the optical switch and optical coupler in the SDM scheme. Y. J. Rao came up with a spatially multiplexed fiber sensing system and realized 32 FBGs multiplexed [20]. The topological structure for SDM is quite complex, and the speed is limited by the optical switch.

2.2 Hybrid schemes of different multiplexing formats

From the above discussion, single multiplexing schemes cannot satisfy the great demand of large capacity and high spatial resolution. Combination of different multiplexing schemes together is an effective way to improve the performances of the FOSN [21, 22]. Here we mainly discuss two hybrid multiplexing schemes for flexible or ultra-large capacity sensor units accessing to the sensor network.

2.2.1 Hybrid sensor passive optic network (HSPON) with flexible access [23, 24]

Most of us are familiar with the topology of fiber to the X (FTTX), which consists of the optical line terminal (OLT), the optical distribution network (ODN), and the active optical network units (ONU). The downstream is broadcasted from OLT to every ONU, while the upstream is directionally transmitted from certain ONU to OLT. According to this configuration, we proposed the architecture of fiber optic sensor PON (SPON), as displayed in Fig. 1. The SPON is also composed of three main parts, including OLT, ODN, and optic sensor units (OSU). However, it is different with the optical communication PON. Firstly, the transmission data

from OLT are always analog and is broadcasted to every OSU from ODN. Secondly, the OSU is always passive due to the characteristics of the optical sensor. Hence, in order to make the SPON work effectively, the OSU should be of self-feedback, i.e. it can reflect the modulated signal which carries the sensing information to the OLT through the ODN, and then the modulated signal can be demodulated at OLT to achieve the sensing parameters. In this network, the OSUs can be multi-functions, multi-structures, and also multi-points, provided that the OLT can provide appropriate light source and signal demodulation processing. Therefore, the SPON is of large capacity, good adaptability, high extendibility, and great flexibility as the fiber communication PON [23].

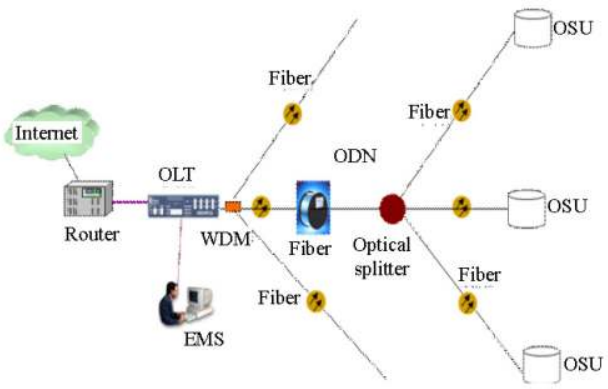

Fig. 1 Schematic diagram of the SPON architecture [23].

Figure 2 presents a typical hybrid TDM/WDM multiplexing SPON (HSPON). The TDM is realized by employing fiber delay lines of different lengths in different links, and the WDM is achieved by the WDM device connected to every OSU. The OLT generates high-power and wideband pulse light, which is transmitted to each OSU through the TDM/WDM distribution network, and then receives the sensing optical signal from OSUs. Assuming that the number of the wavelength channels is m, the number of time-domain channels is n, and the total number of the sensing units is $m \times n$. m is determined by the spectrum bandwidth of super luminescent diode (SLD), and the channel interval of WDM and etc., while n is limited by the power of the light source and the optical link loss. According to the performance of the commercial devices, the capacity of the HSPON can reach 8×32=256 [24]. In this configuration, OSU can be interferometer based vibration sensor, optical spectrum absorption based gas sensor, and Faraday effect based circulator sensor, etc. Therefore, the HSPON can be widely utilized in many application fields such as multi-zone monitoring, multi-parameter detection, and multi-function monitoring [23].

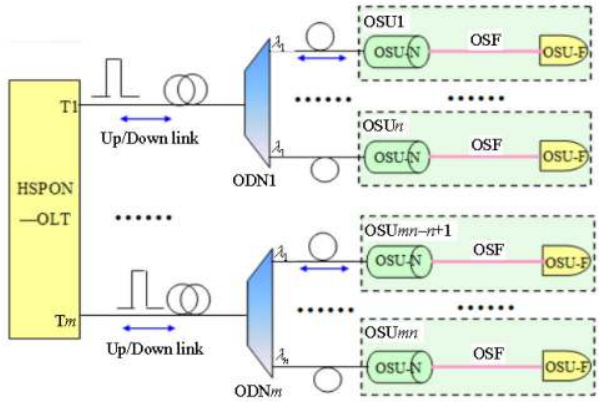

Fig. 2 Schematic diagram of the configuration of the HSPON [24].

2.2.2 Fiber optic microstructure based hybrid WDM/FDM/TDM sensor network with ultra-high capacity access

We further proposed a fiber optic microstructure based hybrid WDM/FDM/TDM sensor network for further expanding the capacity and improving the practicality. The structure and spectral characteristics of the microstructure are presented as Figs. 3(a) and 3(b), respectively [25]. Actually, it is an FP interferometer composed of two closely spaced and identical ultra-short FBGs with ultra-weak reflectivity. Then, the typical spectrum of the microstructure is a low reflective Bragg reflection spectrum modulated with certain resonant periods which is defined as the frequency of the microstructure. It is obvious that the microstructures can be encoded with different wavelengths, frequencies, and time, which are realized by choosing different central wavelengths of FBGs,

different spatial distances between the FBGs pairs, and delay fiber with a certain length. The measurand affected on the microstructure can be demodulated from the wavelength shift of the spectrum. Hence, it has a great potential for large capacity multiplexing by using hybrid WDM/FDM/TDM along a single fiber. As shown in Fig. 3, the microstructures are divided into several time groups through the delay fiber. In every time group, the microstructures are hybrid WDM and FDM. Defining the multiplexing numbers of the WDM, FDM, and TDM as *M*, *N*, and *Q*, respectively, the total network capacity should be *M***N***Q*, which could be significantly enhanced compared with other multiplexing schemes.

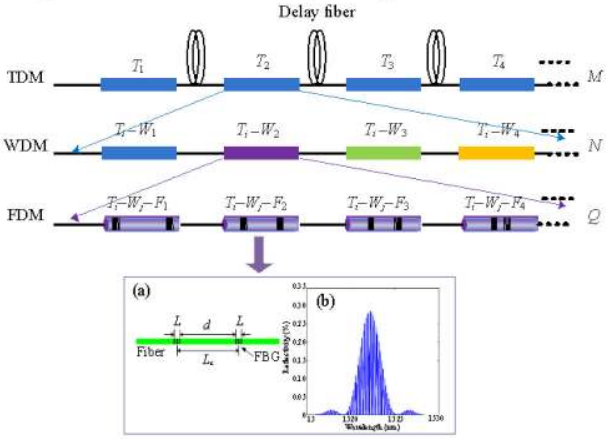

Fig. 3 Schematic diagram of the hybrid WDM/FDM/TDM fiber sensor network [inset: (a) configuration and (b) reflective spectrum of the microstructure].

Assuming that the scanning bandwidth of the system is set as 80 nm from 1510 nm to 1590 nm, the working bandwidth budget of the sensors is optimized to 2.5 nm. Hence, the number of WDM (*M*) will be more than 32. Meanwhile, and there is a trade-off between the TDM and FDM channels, due that more microstructures with FDM in one time group means higher total reflectivity of the group and then will limit the TDM number. Therefore, the optimized capacity of hybrid TDM and FDM, i.e. *N***Q*, could reach to 1000 when the reflectivity of the microstructures is 0.04% [13]. Consequently, the total capacity of the three-dimensional hybrid multiplexing FOSN could be greatly improved to an ultra-large amount of 32000.

3. Specialized light sources for FOSN

3.1 Multi-wavelength fiber lasers operating at C band

Multi-wavelength fiber lasers possess versatile applications in dense WDM systems for expanding the capacity of the sensing network, as well as developing the remote sensing. Appropriate multichannel all-fiber filters play crucial roles in the implementation of multi-wavelength lasing. So far, a lot of all-fiber filters, such as equivalent Lyot birefringent fiber filters [26], fiber Sagnac loop mirrors [27], Mach-Zehnder interferometers [28], Fabry-Pérot filters [29], cascaded long-period fiber gratings [30], and chirped or sampled fiber gratings [31], have been selected as intra-cavity comb filters to successfully achieve stable multi-wavelength lasing oscillations at room temperature.

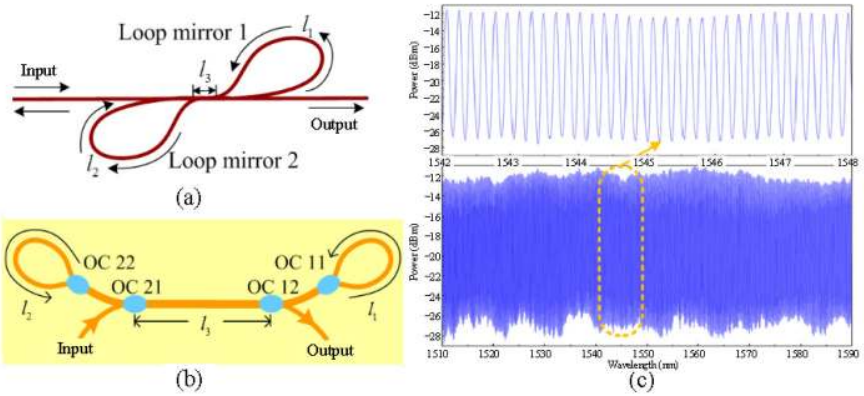

Fig. 4 Characteristics of the MFP: (a) configuration diagram, (b) equivalent model, and (c) comb reflection spectrum [35].

Recently, several kinds of micro/nanofiber (MNF) based fiber lasers have been demonstrated for the miniaturization of fiber-optic components or devices [32−34]. Especially, the microfiber Fabry-Pérot (MFP) filter acting as a comb filter paves another way to implement multi-wavelength lasing. Figures 4(a) and 4(b) show the configuration diagram and equivalent model of the MFP, respectively, where the coupling regions can be regarded as optical couplers (OCs) owing to the evanescent coupling between adjacent microfibers. Benefiting from the all fiber and compact size of the Sagnac loop mirror structure, the MFP presents excellent comb filtering spectrum as depicted in Fig. 4(c), with high extinction ratio of about 15 dB, narrow 3 dB linewidth of each channel of only 55 pm, and the channel flatness better than 2 dB within the broad bandwidth from 1510 nm to1590 nm [35].

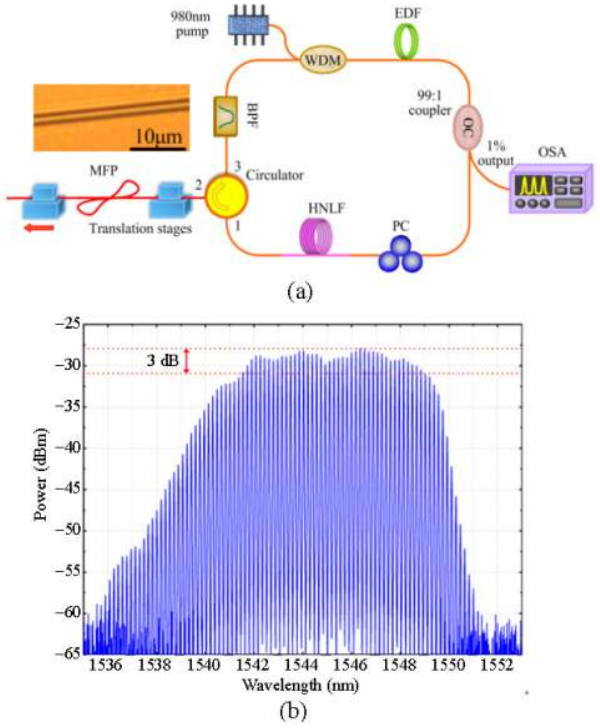

Fig. 5 Characteristics of the MFP based fiber laser: (a) schematic of the multi-wavelength fiber laser [inset: micrograph of the microfiber and (b) typical multi-wavelength lasing output [35, 36].

The corresponding multi-wavelength fiber laser is schematically depicted in Fig. 5(a), where the MFP is served as the multi-wavelength selector and highly non-linear fiber (HNLF) is utilized to suppress the mode competition induced by the erbium doped fiber (EDF). A typical multi-wavelength lasing output is illustrated in Fig. 5(b). Up to 42 simultaneously lasing wavelengths with a wavelength spacing of 0.18 nm are obtained. The 3 dB linewidth of each channel is about 25 pm, and the side-mode suppression ratio (SMSR) is more than 35 dB [35]. Further, by moving the translation stages to mechanically adjust the cavity length of the MFP, the wavelength-spacing as well as the channels-numbers of the multi-wavelength laser can be continuously tuned [36].

3.2 Switchable and tunable multi-wavelength fiber lasers operating at the 2 μm region

Recently, interest of operating wavelength among fiber lasers has been transferred from C band and L band to the 2 μm region, for the reason that infrared fiber lasers demonstrate intriguing advantages in atmospheric transmission, hydrocarbon gas sensing, laser lidar, and eye safety [37, 38].

Additionally, switchable and tunable multi-wavelength fiber lasers mainly employ overlap cavities or polarization hole burning (PHB) to control or adjust the properties of wavelength and therefore to achieve wavelength switching. According to the two basic theories, various methods have been proposed and reported, such as cascaded FBGs [39], highly birefringent (Hi-Bi) fiber loop mirrors [40], Sagnac loop mirror [41], fiber Bragg gratings (FBGs) written in Hi-Bi fibers [42, 43], and acoustic waves [44]. In the following, two typical kinds of switchable and tunable multi-wavelength fiber laser operating at the 2 μm region, which adopt the above methods in the Tm-Ho co-doped fiber laser (THCDFL), are introduced.

3.2.1 Design of the Sagnac loop as the comb filter [45]

Figure 6 illustrates the simple configuration of multi-wavelength lasing based on the Sagnac comb

filter and Tm-Ho co-doped fiber (THCDF) coiling round the plates of three-loop polarization controller (PC), where the comb filter is a Sagnac loop mirror composed of a piece of polarization maintaining fiber (PMF) and a 3 dB coupler. The polarization hole burning can be obtained without polarization maintaining-Tm-Ho co-doped fiber (PM-THCDF) and avoids the splice loss between the PM-THCDF and single mode fiber. The comb filter which consists of PMF and PC is effective to suppress the wavelength competition at room temperature. Tunable multi-wavelength lasing of different positions can be achieved by simply adjusting PC.

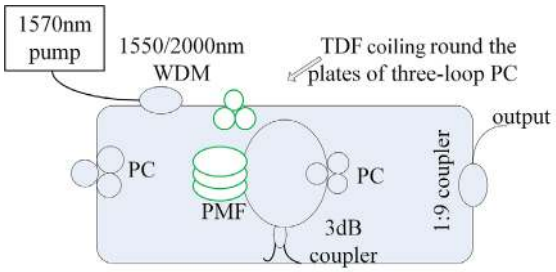

Fig. 6 Schematic of the proposed multi-wavelength THCDF laser based on the Sagnac comb filter [45].

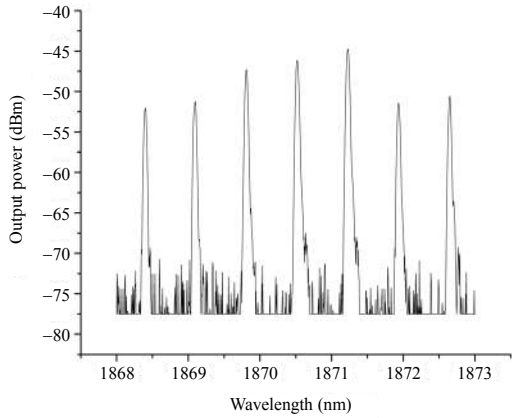

Fig. 7 Spectra of the multi-wavelength lasers with PMF [45].

Figure 7 presents the spectrum of the multi-wavelength lasers with PMF. It can be seen that stable seven wavelengths with the smallest wavelength spacing of 0.65 nm are obtained. The shortest and longest wavelengths are 1868.4 nm and 1872.7 nm, respectively. The SMSR is about 35 dB with the maximum peak power of −53 dBm at around 1871.2 nm. The number of the wavelength and the channel spacing can be tuned by adjusting the angle of PC, for changing the birefringence and phase difference in the Sagnac loop.

3.2.2 Design of the parallel cavities based on 3×3 coupler [46]

The configuration of the switchable and tunable dual-wavelength fiber laser at the 2 μm region is schematically shown in Fig. 8. The laser topology is based on the parallel connection of FBGs using a 3×3 coupler which acts as two individual cavities, so that the dual wavelengths are tunable and switchable by adjusting the central wavelength of FBGs and the cavity losses.

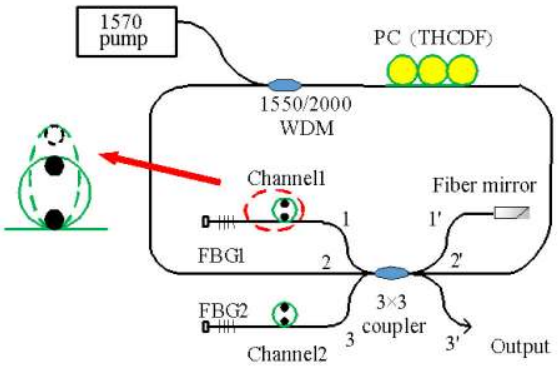

Fig. 8 Configuration of the switchable and tunable dual-wavelength fiber laser around 2 μm [46].

The dual wavelengths enjoy the same gain medium by the parallel connection of FBGs. Introducing lower losses for one wavelength will cost some gain for another wavelength, and thus, the output laser can be switched from one wavelength lasing to another or dual-wavelength lasing together by adjusting the variable attenuator (VA) and pump power. Figure 9 shows the laser operating in switching mode.

The dual-wavelength of this laser is dependent on the central wavelengths of the FBGs. Changing the central wavelengths of the FBGs by strain or temperature will tune the wavelength of output laser. Figure 10 shows the tunability of the laser by strain tuning the FBG1 and FBG2 individually. Tuning ranges of 6.5 nm (1890.6 nm – 1897.1 nm) and 4 nm (1919.4 nm – 1923.4 nm) are obtained, respectively.

The period and the reflectivity of FBGs will be changed when tuning the central wavelengths of the FBGs by strain.

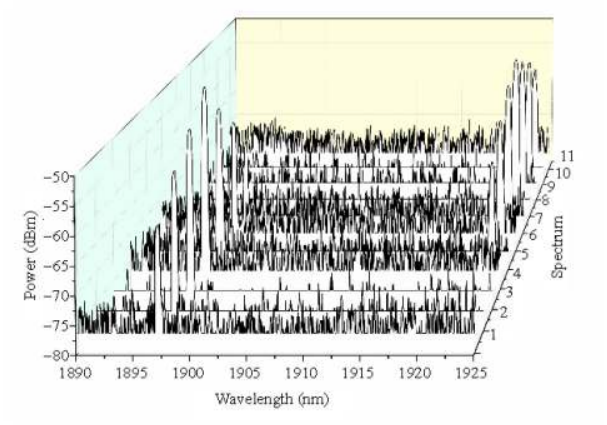

Fig. 9 Output spectra when laser operates in the switching mode [46].

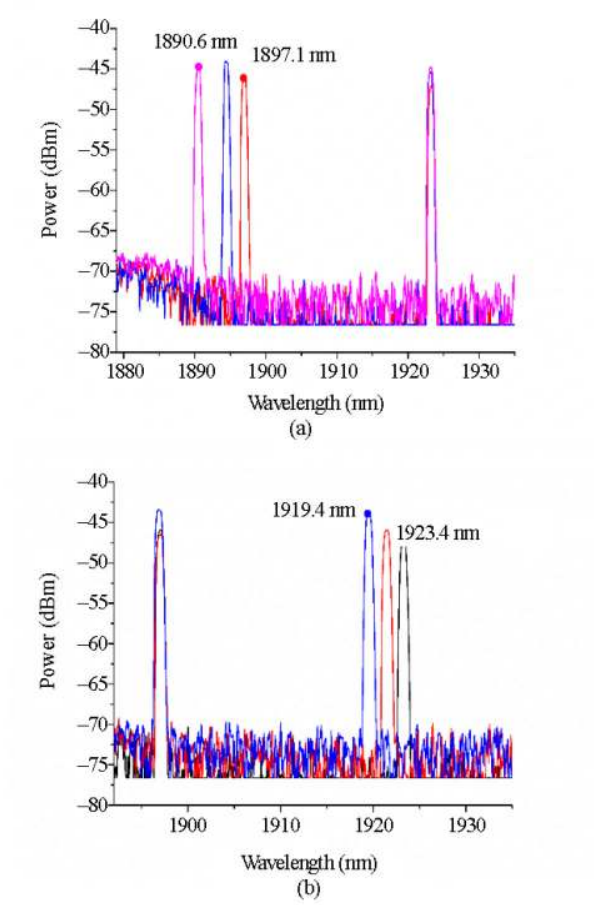

Fig. 10 Output spectrum of the dual-wavelength fiber laser when strain tuning the (a) FBG1 and (b) FBG2 [46].

3.3 Ultra-fast mode-locked fiber lasers

Mode-locked fiber laser has the potential for a spectrally bright pulsed broadband source that can be used for interrogating in the fiber sensor network. The light source is made from relatively low-cost fiber-pigtailed off-the-shelf components and does not require an optical modulator to achieve ultra-short light pulses [47]. Thus far, single-wavelength ultrafast fiber lasers have been investigated theoretically and demonstrated experimentally [48−52].

Multi-wavelength mode-locked fiber lasers have also been widely explored by using actively and passively mode-locked mechanisms in different wavelength regimes (1 μm, 1.5 μm, and 2 μm) [53−57]. Compared with the actively mode-locked fiber lasers, passively mode-locking fiber lasers are technically easy to operate and compact in structure as well as has low jitter in performance. Recently, mode-locked fiber lasers have attracted a great deal of interest due to their compact size and high flexibility for both pulse width and repetition rate. Therefore, this kind of fiber lasers possesses a flexible application in the TDM-based sensing network. Especially, the ultrashort pulse width contributes to the improvement in the spatial resolution.

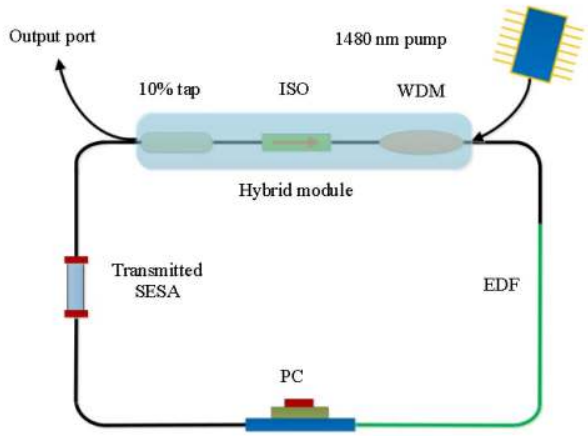

Fig. 11 Schematic of the passively mode-locked fiber laser [58].

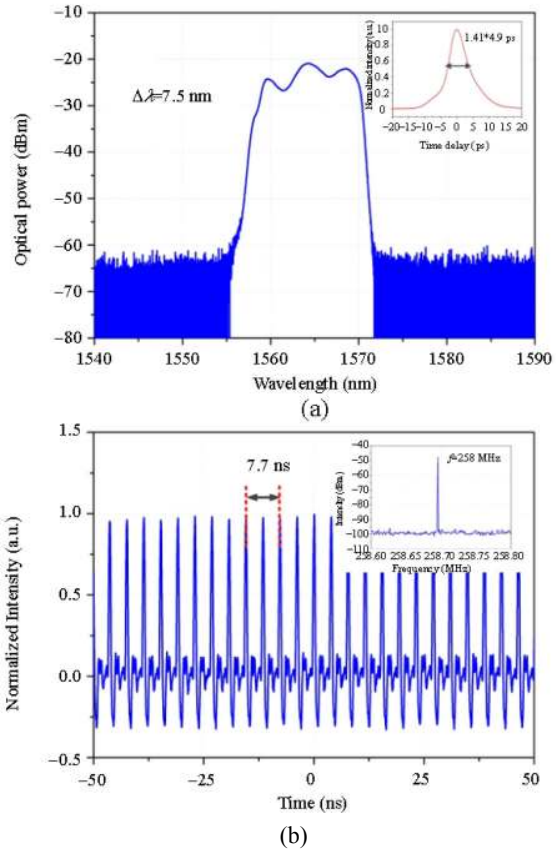

Fig. 12 Characteristics of the passively mode-locked fiber laser: (a) optical spectrum of the 2nd-order harmonic mode-locked DSs [inset: the corresponding autocorrelation trace] and (b) corresponding oscilloscope trace [inset: the RF spectrum] [58].

High repetition rate dissipative soliton (DS) pulses are generated in the normal-dispersion erbium-doped fiber lasers mode-locked by a transmitted semiconductor saturable absorber (SESA), as schematically depicted in Fig. 11. The wavelength division multiplexer/isolator/tap hybrid module (WDM/isolator/tap hybrid module) plays a crucial role in shortening the cavity length for achieving a high fundamental repetition rate. As a result, through tuning the pump power and appropriately adjusting the intra-cavity polarization state, 2nd-order harmonic mode-locked DS pulses are obtained as illustrated in Fig. 12. The rectangular optical spectrum of these DS pulses is shown in Fig. 12(a) with a 3-dB bandwidth of 7.5 nm, and the autocorrelation trace depicted in the inset declares a pulse width of 4.9 ps if a Gaussian pulse shape is assumed. Thus, the time-bandwidth product is 4.6, indicating that these DS pulses are strongly chirped. Figure 12(b) and its inset show the oscilloscope trace and radio frequency (RF) spectrum, respectively. The harmonic repetition rate is fixed at 258 MHz, and two pulses coexist in a cavity round-trip interval of 7.7 ns, which agree well with the cavity length. The average output power of fundamental mode-locking is around 6.6 mW with the pulse energy of 25.5 pJ. The strongly chirped pulses could be potentially compressed to femtosecond pulses through chirp compensation, which provides a possibility for achieving ultrashort pulsed light source with high repetition rate [58].

3.4 Optical broadband chaos

Optical chaos has been widely applied to fiber fault monitoring [59−61] and fiber sensing [62−66]. The study of optical chaos has lasted for nearly half a century. By introducing an optical feedback into a semi-conductor laser, the laser output is no longer stable, but it shows the property of small random fluctuation in intensity, wavelength, and phase, i.e. chaotic state. With the noise-like property, the correlation of optical chaos has the characteristic of Dirac function, making it extremely suitable for applications in fiber fault locating. Moreover, as the amplitude of the correlation is determined by the intensity of the optical chaos, intensity demodulation in fiber sensing networks can also be achieved at the same time.

The experimental setup of an optical broadband chaos is shown in Fig. 13. A semiconductor optical amplifier (SOA) ring structure with an isolator (ISO) acts as the chaotic light source. The SOA has the parameters of central wavelength (1500 nm), optical bandwidth (74 nm), saturation output power (14 mW), and the small signal gain (13 dB). The 80:20 optical coupler (OC1) provides 20% feedback and 80% output. The polarization controller (PC) is used to adjust the polarization of the light into the SOA, and the erbium doped fiber amplifier (EDFA) can enhance the power of output chaos. A 99:1 optical

coupler (OC2) provides 1% transmission light as the reference signal and 99% transmission light as the detected signal. The circulator assures that the return signal can be detected. Two photon detectors (PDs) with 1 GHz bandwidth are used in the correlation detection [61, 65].

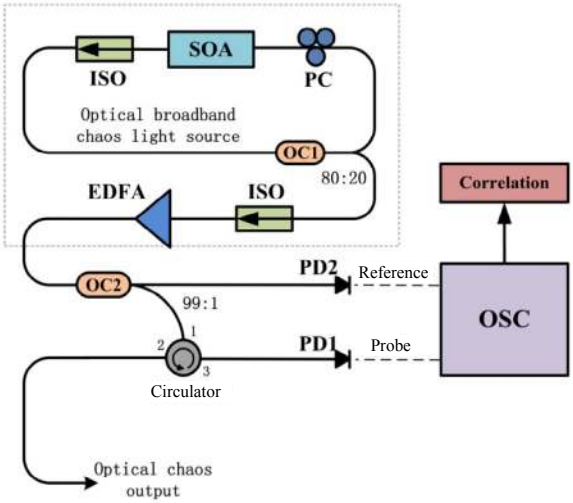

Fig. 13 Schematic diagram of the proposed optical broadband chaos [65].

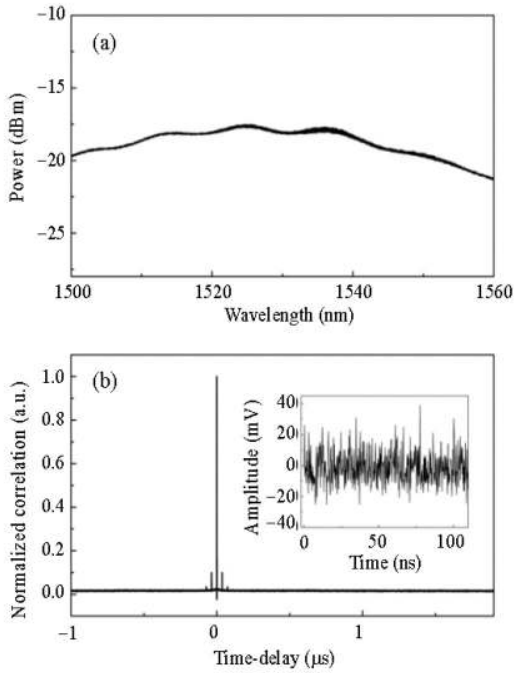

Fig. 14 Characteristics of the broadband chaotic source: (a) the optical spectrum and (b) the autocorrelation curve [inset: the time series] [65].

An optical spectrum analyzer (Yokogawa AQ6370C) and a radio frequency (RF) spectrum analyzer (Agilent 40GHz E4447A) are used to observe the chaotic output light. A real-time oscilloscope (OSC) with 12.5 GHz bandwidth and 50 GSa/s sampling rate is used to record the reference signal and reflected signal. At last, the data recorded in the OSC are processed by the cross correlation method. The characteristics of our proposed optical broadband chaos are demonstrated in Fig. 14(a) with a high quality of autocorrelation curve in Fig. 14(b) (inset: the time series).

4. Intelligent management for FOSN

4.1 Demodulation techniques for FOSN

The demodulation technique is critical for the fiber sensing network to extract the sensing parameters. As the optical spectrum includes comprehensive information such as the wavelength, intensity, and repetition period, the wide bandwidth, high resolution, and high speed optical spectrum scanning are the most important. The most common way to demodulate the spectrum is based on the charge coupled device (CCD) or tunable FP filter. The CCD module has a relatively high acquisition speed up to 3.5 kHz and is suitable for a low light detection. But the physical resolution is limited by the diffraction part to only 20 pm and the integration time limits the speed of the demodulation [67, 68]. The tunable FP filter can be configured flexibly and achieve a high resolution up to 1 pm. However, the FP filter is easy to be affected by temperature fluctuation [69, 70]. Another ultra-high resolution demodulation scheme is the coherence spectrum analysis [71], while the total processing time for the narrow wavelength band will be as long as tens of seconds, which is not suitable for dynamic sensing. In the following, we will present a flexible, wide bandwidth, high resolution, and high speed demodulation scheme for the hybrid multiplexed FOSN.

Figure 15 depicts the composition of the demodulation module. Light from the broadband

light source is modulated into pulse by the acoustic optical modulator (AOM) and then transmits to the sensing fiber through the circulator. The light pulse reflected from the microstructure is first amplified by the EDFA, then passes through the tunable FP filter, and finally detected by the high speed avalanche photodiode (APD) detector with the rise time of only 300 ps [72, 73]. To guarantee the synchronization of the AOM, the tunable FP filter, and the analog-to-digital (AD) data acquisition, all of them are driven by the same field programmable gate array (FPGA) card [73]. A symmetrical triangular signal composed of multiple steps is utilized to control the tunable FP filter, which could ensure stable transformation of the driving signal. As a result, the light intensity of different time groups corresponding to certain driving signals, i.e. wavelength, can be obtained. For accurate demodulation, a tunable laser is employed to calibrate the function of the driving signal-wavelength curve in advance. In addition, a compensating weak FBG isolated from the strain is adopted to eliminate the spectral drift of the FP filter induced by the environment temperature variation through the real-time wavelength calibration, which is beneficial for high accurate and stable demodulation. Based on the above demodulation principle, there is trade-off between the scanning bandwidth and the wavelength resolution, due that the ratio of the bandwidth to the resolution equals to the number of the sampling points. Therefore, the demodulation performance could be flexibly controlled according to the application requirement.

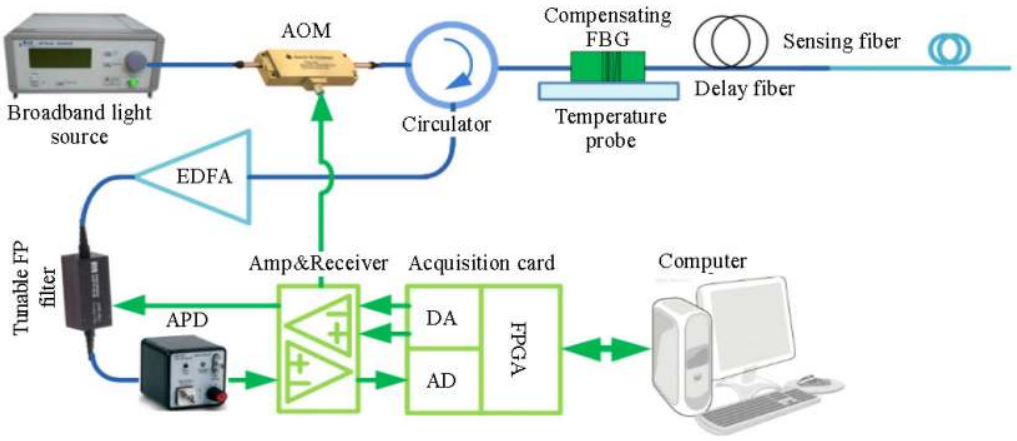

Fig. 15 Schematic diagram of the demodulation module for the hybrid fiber sensor network.

An NI Data acquisition platform is utilized to build the demodulation module. Taking the hybrid WDM/FDM/TDM fiber sensor network discussed in Section 2.2.2 as an example, the demodulation performance is investigated. Figure 16(a) presents the wavelength tracing results of a tunable laser from 1511 nm to 1585 nm, which demonstrates that the scanning bandwidth of the demodulation module is beyond 75 nm. To test the wavelength resolution, we heat the sensing microstructure from 24.2 ℃ to 24.3 ℃, and then it is clear that the peak wavelength changes from 1540.151 nm to 1540.152 nm as shown in Fig. 16(b), which proves that the wavelength resolution is higher than 1 pm. Figure 16(c) displays the driving signal of the FP filter with each step taking 0.5 μs. For the occasion of the 20 nm bandwidth and 5 pm resolution, the sample points could be decreased to 4000. Then, each sweeping cycle will take only 2 ms, corresponding to a high sweeping speed of 500 Hz. In general, a flexible

demodulation platform with the maximum bandwidth over 75 nm, high wavelength resolution up to 1 pm, and fast sweeping speed of 500 Hz can be realized for hybrid multiplexed FOSN.

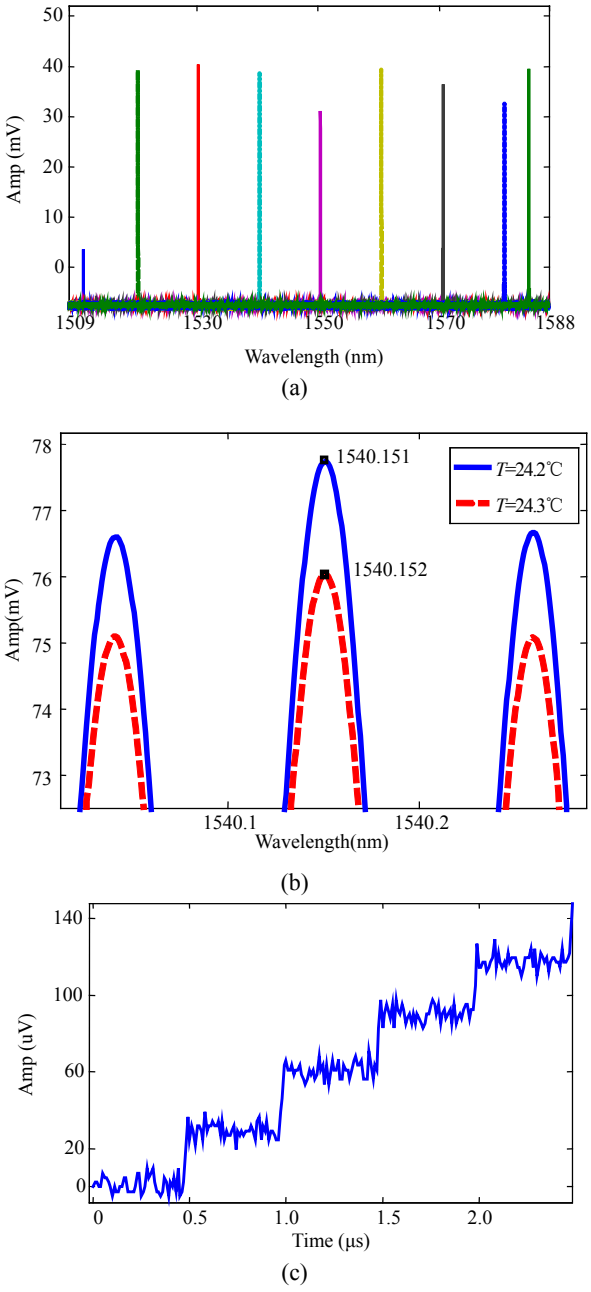

Fig. 16 Demonstration of the demodulation performances: (a) wavelength scanning of a tunable laser, (b) recovered spectrum for 1pm wavelength shift, and (c) fast driving signal of the FP filter.

4.2 Fault monitoring of the fiber transmission link in FOSN

The survivability of the FOSN in harsh environment can not be ignored in practical applications, where the most important for intelligent management is the real-time fault monitoring and locating in the fiber transmission link of the FOSN. Specifically, the detection of faults in fiber links at different wavelengths is urgently required to guarantee the reliable operation of the WDM FOSN. Conventional optical time domain reflectometry (OTDR) has difficulty in diagnosing the faults in a WDM-PON due to its fixed wavelength probe light [74]. Although a wavelength tunable sequence OTDR has been recently reported, without an expensive highspeed sequence generator and a wideband modulator, its resolution is still limited to tens of meters [75].

In order to locate simultaneously and precisely the faults among all fiber links in an FOSN, we provide a simple solution based on optical wideband chaos. Take a large capacity FOSN with hybrid TDM and WDM as the example. The schematic diagram of the large capacity quasi-distributed sensing network is shown in Fig. 17. Chirped fiber Bragg gratings (CFBG) based intensity demodulation is implemented by the programmed optical band pass filter (OBPF, Waveshaper, and FINISAR), which slices optical broadband chaos into multi-wavelength channels in consistent with the CFBG sensors [76].

A cross-correlation algorithm is applied to the chaotic reference signal and probe signal to interrogate the measurand sensing and the precise locating of each sensor. Meanwhile, the fiber breakpoint location can be also achieved through processing the reference signal and the Fresnel reflection signal of the fiber fault based on the same principle [61]. A proof-of-concept experiment is conducted with six CFBG sensors (S11, S12, S13, S21, S23, and S32) deployed in three sensing fiber lines. Three wavelength channels are filtered by the OBPF in consistent with the CFBG sensors, and an additional channel (testing channel) of 2.4-nm (300-GHz) bandwidth is reserved to provide

sufficient optical power for fiber fault monitoring, as depicted in Fig. 18 [76].

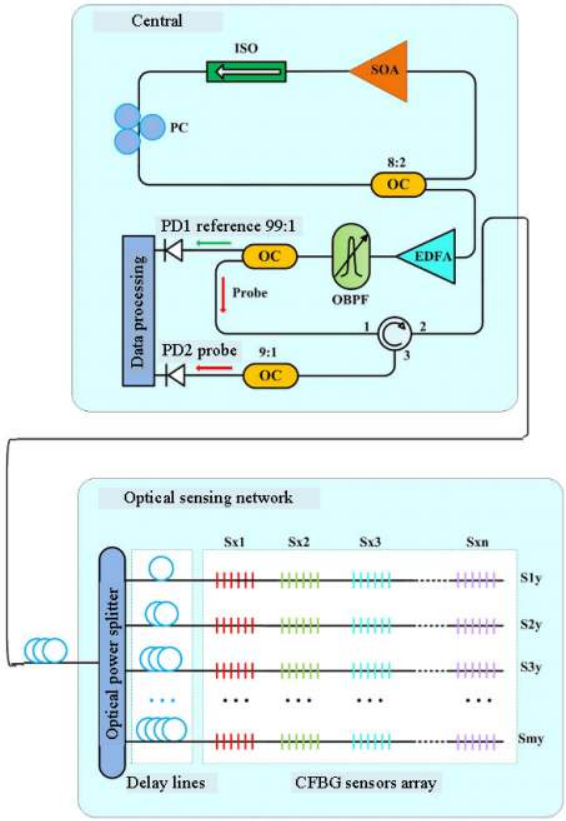

Fig. 17 Schematic diagram of the large capacity quasi-distributed sensing network [76].

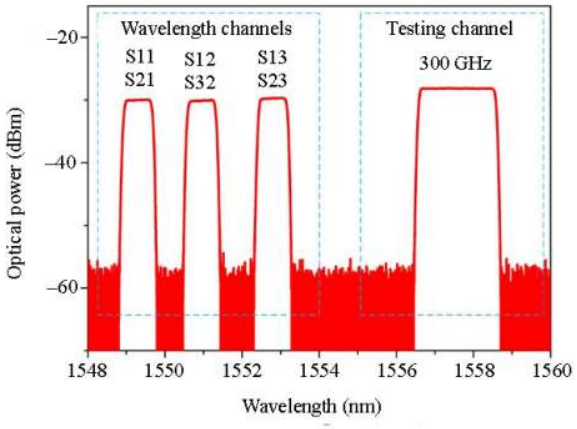

Fig. 18 Optical spectrum of the multichannel chaos, including three wavelength channels and a testing channel [76].

When strain is applied to a certain CFBG, the amplitude of the corresponding correlation peak will decrease due to a decrease in the reflection intensity. When a breakpoint occurs in the sensing network, an extra correlation peak will appear in the correlation spectrum, and its position indicates the location of the breaking point. Figure 19 presents the experimental results of simultaneously three fault points in different sensing lines, respectively. Through the peak searching algorithm, precise locating of the breakpoints can be pinpointed with a spatial resolution of 2.8 cm [76].

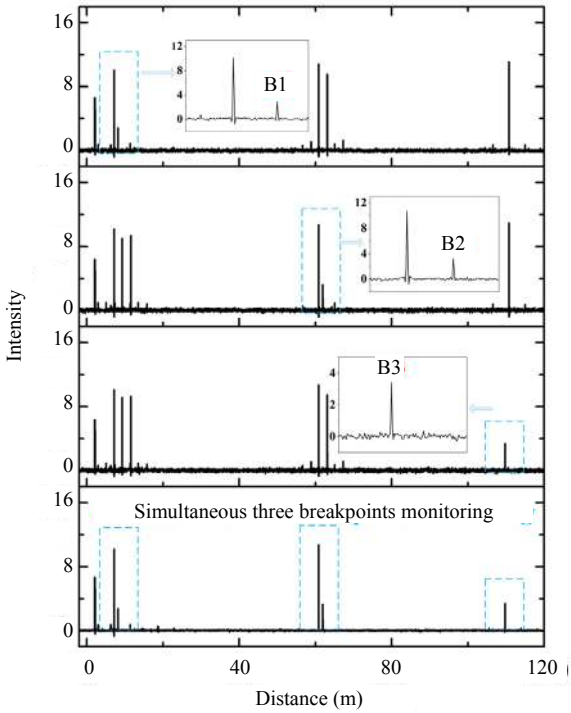

Fig. 19 Experimental results of the real-time fiber fault monitoring [76].

5. Fiber optic gas sensing structures and networks

Fiber optic gas sensors have intrinsic benefits over conventional dielectric and semiconductor sensors, as they are immune to electromagnetic interference, safe in dangerous or hazardous environments, and furthermore facilitate remote and distributed sensing. Numerous techniques are investigated for optical gas sensing. For instance, techniques based on spectrum absorbing including non-dispersive infrared (NDIR), tunable diode laser spectroscopy (TDLS), cavity ring-down spectroscopy (CRDS) as well as photo-acoustic

detection (PAS) have been demonstrated [77]. In this section, research progress on special fiber optic structures designed for gas sensing, realizations of optical gas sensing systems by combination the fiber optic sensors and optical networks, and typical practical applications and demonstrations of fiber optic gas sensing networks are reviewed.

5.1 Engineered fiber optic gas sensing structures

Novel fiber structures such as surface processed fibers with sensitivity enhancement, fiber gratings, and photonic crystal fibers can be employed as gas sensors due to the evanescent field of the core mode. For gas absorption measurement, the evanescent field has to be extended to penetrate the external environment to provide interaction between the guided light and the external gas [78].

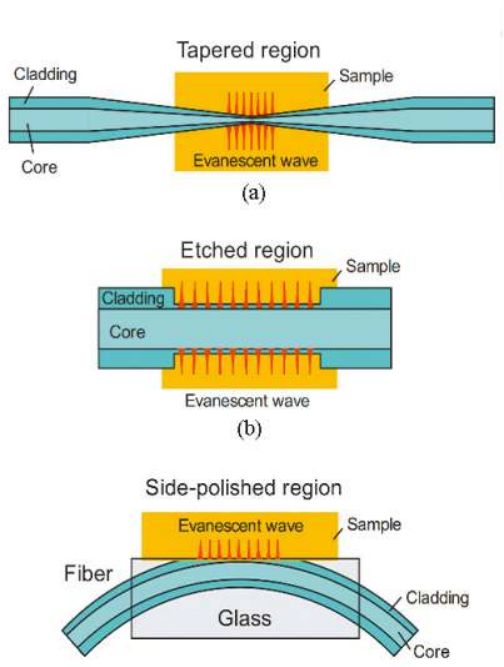

Fig. 20 Scheme diagrams of (a) tapered fiber, (b) etched fiber, and (c) side-polished fiber [78].

Specific fiber surface processing techniques have been adopted, including tapered fiber, etched fiber, and side-polished fiber, as illustrated in Fig. 20. These different types of sensor elements are used in fiber-cavity ring-down spectroscopy for gas sensing [78].

Micro/nano fiber (MNF) with the sub-wavelength diameter is also a good candidate for gas sensing. By using a graphene coated micro fiber, an all-fiber ammonia gas sensor can be realized, as shown in Fig. 21. The microfiber is bilaterally stretched from a standard single mode fiber (SMF) by employing the flame heating and taper-drawing technology. Graphene is coated on the microfiber by pump light induced deposition, which improves gas sensitivity through its significant high specific surface area to attract gas molecules and thus achieve a resolution of 0.74 ppm in the ammonia gas detection [79].

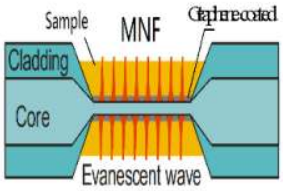

Fig. 21 Structure of graphene coated micro/nano fiber served as the ammonia gas sensor.

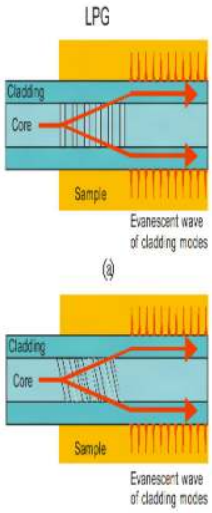

Fig. 22 Scheme diagrams of (a) LPG and (b) TFBG [78].

Fiber gratings have similar advantages along with the surface processed fiber sensor in stability and establishing fiber networks. Evanescent waves of cladding modes of the fiber grating interact with

the surrounding medium, which leads to the change in the resonant wavelength. Most used fiber gratings are long period grating (LPG) and tilted FBG (TFBG) [78, 80], as presented in Fig. 22.

The holes in the photonic crystal fiber (PCF) can also be utilized as convenient repositories for gases. A significant overlap between the physical location of the holes and the guided modes leads to strong interaction between the two and allows great potential for gas sensing. The PCF is extremely potential for being a long path length, and low volume gas cell, which can bring big benefit in enhancing sensitivity from the Bear-Lambert law. Nevertheless, one of the main challenges of using these PCF gas cells is the effort to fill the PCF with the target gas [81]. Techniques to improve the sample filling time include increasing the pressure difference across the fiber and increasing the cell diameter or introducing holes to allow gas flow or diffusion along the waveguide's length [82], as illustrated in Fig. 23. For example, Parry's group has reported a methane sensor with 500 ppm detection limit by using a 10 μm core photonic band-gap fiber (PBGF) operated at 1.650 μm [83].

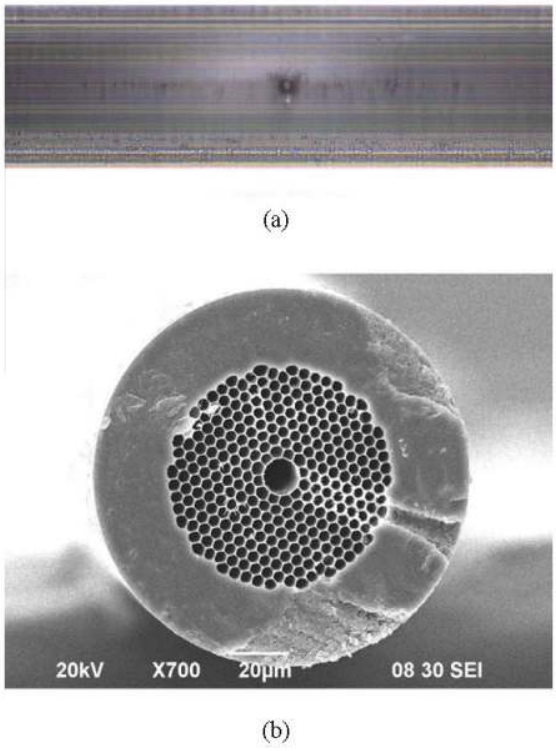

Fig. 23 PBGF images for gas detection: (a) side-view and (b) cross-section of a micro channel fabricated on the hollow core PBGFs (HC-PBGFs) [81].

5.2 All fiber optic gas sensing networks

In many occasions, the multipoint gas sensing network is desired to obtain a large-scale gas distribution and reduce the cost per sensing point. This can be realized by the combination of fiber optic sensors and fiber optic networking technologies. In order to accurately and effectively detect the multipoint data, versatile multiplexing techniques have been developed, such as spatial SDM [84], TDM [85], frequency division multiple access (FDMA) [86], frequency modulated continuous wave (FMCW) [87], synthesis of optical coherence function (SOCF) [88], and WDM [89]. These techniques own unique features. For example, For FWCW, the laser source needs intensity modulation, and the complex system requires the voltage controlled oscillator and RF mixer. For SOCF, only one sensor can be measured each time, and the location resolution is limited by the coherent length of the laser [88].

Recently, based on TDLS and TDM techniques, commercial products named OptoSniff® as fiber optic gas sensing networks are presented by the OptoSci Ltd [90]. The overview of the system is schematically shown in Fig. 24, including the central control unit (CCU), fiber optic network composed of power splitters and optical multicore cables, and all-optical gas sensing cells. Due to the benefits of optical fiber networks and passive devices, it offers continuous, multipoint methane/natural gas leak detection and monitoring, from hundreds of sensing points (240 points) over a long distance (20 km). These products have been applied in British landfills and Japanese Tokyo gas service tunnels, monitoring methane and carbon dioxide, lasting for over 2 years. This is a typical case and major breakthrough for the practical applications of all-fiber optic gas sensing networks.

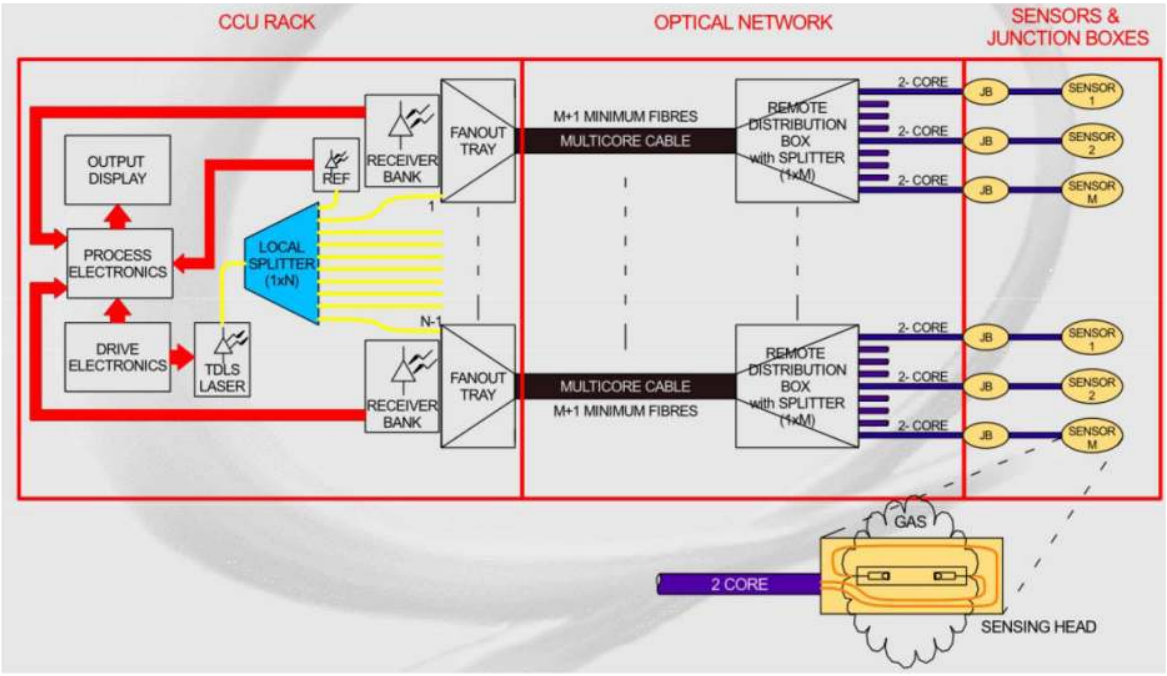

Fig. 24 Schematic diagram of the OptoSniff® multipoint fiber optic gas sensing system [90].

6. Fiber optic acoustic sensors for the sensing network

Acoustic sensors have been studied extensively for decades and play an important role in the modern society. The acoustic wave has a wide frequency spectrum range that extends from infrasound (<20 Hz) up to ultrasound (in the GHz-band), and different frequency bands have different sensing applications [91]. For the unique advantages of large bandwidth, high sensitivity, immunity to electromagnetic interference, remote detection, and multiplexing capability, fiber optic acoustic sensors can break the limitations of traditional electric acoustic sensors [92]. Currently, numerous fiber optic acoustic sensors have been researched, of which the configurations are based on fiber optic interferometers such as Mach-Zehnder, Michelson, Sagnac, Fabry-Pérot, or FBGs [93], and also some special structures such as fiber lasers [94], couplers [95], and tapers [96].

The low-frequency acoustic wave detection is of great significance because of its wide applications in the fields of early warning of natural disasters such as earthquakes [97]. However, little work has been done on the research of the optical acoustic sensor for the low-frequency acoustic detection. In order to offer the fiber acoustic sensors with higher sensitivity, good low-frequency response, and easy networking, we have designed several kinds of fiber acoustic sensors, such as intensity modulated sensors with the single-mode/multimode fiber coupler, wavelength modulated acoustic sensor based on dual FBGs, and beat-frequency modulated sensor based on multi-longitudinal mode fiber laser.

6.1 Intensity modulated acoustic sensors [98]

Intensity modulated acoustic sensors can detect the acoustic signal by the changes in the optical intensity directly without the high cost and complex demodulation system, which can be easily used in the FOSN through TDM and SDM. One typical scheme is based on the non-standard fused single-mode/multimode fiber coupler and aluminum foil. For a fused 2×2 single-mode fiber coupler, the coupling ratio (CR) of two output ports is dependent

on the distance (d) between centers of two optical fibers as shown in Fig. 25 [98]. When the acoustic pressure is applied on the foil, the deformation of foil will cause the d change of the fused coupler as shown in Fig. 26. Hence, the acoustic vibration can be measured by detecting the insertion loss of the non-standard fused coupler. Figure 25 implies that the "coupling cycle" shortens with a decreasing in d (from right to left of the horizontal axis), so as the number of coupling cycle increases, the sensitivity of the multi-cycle fused coupler based sensors can be improved. This assumption is experimentally conformed with result of 0.18 mW/Pa (1 cycle), 0.65 mW/Pa (3 cycles), and 1.71 mW/Pa (5 cycles), respectively.

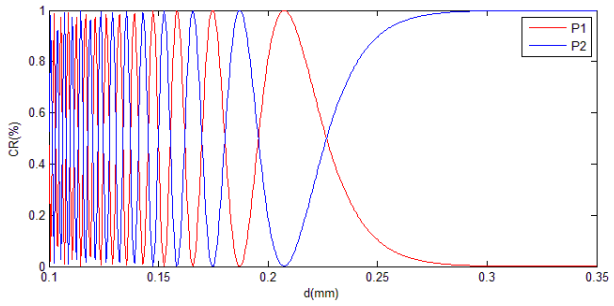

Fig. 25 Simulation of the relationship between CR and d during the fused process [98].

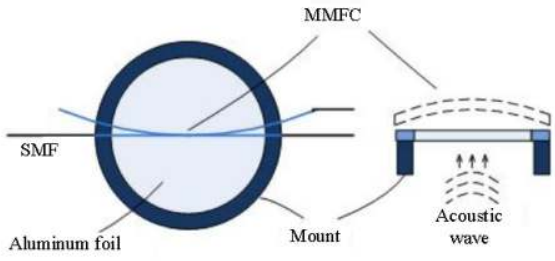

Fig. 26 Sensing mechanism of the fused coupler based acoustic sensor [98].

Moreover, the multimode fused coupler based sensor also has been studied which shows a sensitivity of 2.63 mW/Pa, with the operation frequency range from 20 Hz to 20 kHz and average SNR about 20 dB.

6.2 Wavelength modulated acoustic sensors [99]

Wavelength modulated acoustic sensors are suitable for WDM. An acoustic sensor based on dual FBGs and a titanium film is proposed and experimentally demonstrated, where the sensing head is manufactured by longitudinally sticking one end of each FBG to the titanium film as illustrated in Fig. 27 [99]. One of the two FBGs is employed for transmitting light, and the other is employed for reflecting. The dual FBGs are not only working as the signal transmission line but also as the sensing component. Due to the wavelength shift of the FBGs induced by the external acoustic vibration, the corresponding periodic fluctuation in power can be observed on the optical oscilloscope. The optical fiber sensor shows a relatively flat frequency response in the range from 100 Hz to 1 kHz with the average signal-to-noise ratio (SNR) above 22 dB. In addition, the maximum sound pressure sensitivity of the proposed sensor is found to be 90 μW/Pa within a sound pressure range 100.3 dB – 118.5 dB. The sensing system presents good stability and reliability, and has the advantage of direct self-demodulation.

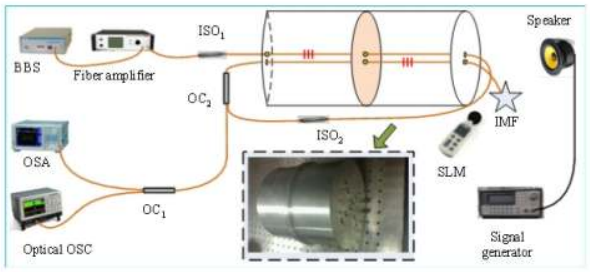

Fig. 27 Schematic diagram of the acoustic sensor based on the dual FBGs and a titanium film [99].

6.3 Beat-frequency modulated acoustic sensors [100]

The passively mode-locked technique which employs carbon nanotubes (CNT) is a widely used method for mode locking and frequency stabilization. The unique frequency stability can be also used for the acoustic pressure measurement [100]. The polymer membrane is employed beneath the pre-strained Er^{+} doped fiber (EDF) to convert the sound pressure disturbance into axial strain, alter the

cavity length, and induce shift of the longitudinal modes beat as displayed in Fig. 28. Hence, the acoustic pressure measurement can be carried out by detecting the shift of beat frequency. The sensor shows comparable strain and sound pressure sensitivity of 0.5 kHz/με and 147.2 Hz/Pa, respectively. The sensor can be an alternative to measure acoustic pressure with good stability, as well as a valuable candidate for the FOSN.

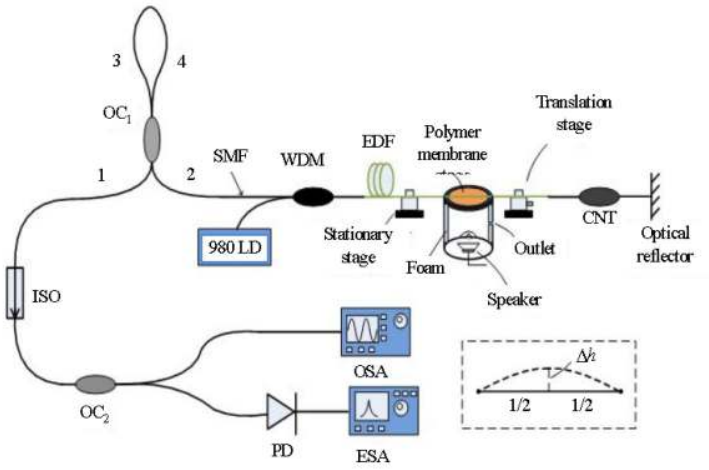

Fig. 28 Schematic diagram of the passively mode-locked multi-longitudinal mode fiber laser sensor [100].

7. Fiber optic static/dynamic strain sensing network

Fiber sensor networks have been widely used in health monitoring of civil and mechanical structures due to their advantages over electrical sensing devices, such as electric insulation and immunity to electromagnetic interference. Meanwhile, the research and application of optical chaos have attracted more and more attention of researchers recently. In the following, we mainly introduce an FBG sensor network for static/dynamic strain sensing. By adopting the optical wideband chaos described in Section 3.4 as the light source, the location of sensing FBGs can be distinguished by the different peak positions along the correlation spectrum, which means that the identical FBGs can be adopted in the quasi-distributed sensing network, which will increase the network multiplexing capabilities [65].

The WDM based multi-point static strain sensing setup is constructed with a 100-GHz-spaced WDM device with 2 channels (CH33 and CH34) and the corresponding sensing grating at each branch, as shown in Fig. 29. The WDM device acts as a band pass filter. The reflection spectrum of the corresponding sensing grating is chosen to match the transmission spectrum of WDM. In the initial, the reflection intensity will get almost 100% reflection after the combined filtering from the WDM and the grating, if we ignore the insertion loss of WDM. When the strain is applied, the wavelength of the grating will shift towards the longer wavelength. Thus, the wavelength spacing between the WDM and the sensing grating will lead to a decrease in the reflection intensity. As we know, when the intensity of optical chaotic reflection changes, the amplitude of peak in the correlation spectrum will also change after the cross correlation calculation. In this way, strain is demodulated from the amplitude of the correlation peaks. In addition, the position of correlation peaks suggests the location of the gratings, thus strain sensing and locating can be achieved at the same time. The correlation spectrum with and without strain applied is shown in Figs. 30(a) and 30(b) [65].

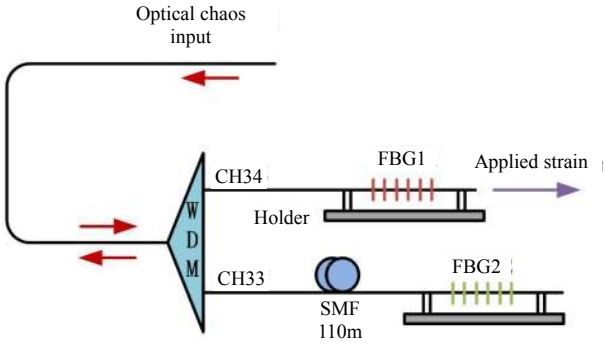

Fig. 29 Schematic of the static strain sensing setup [65].

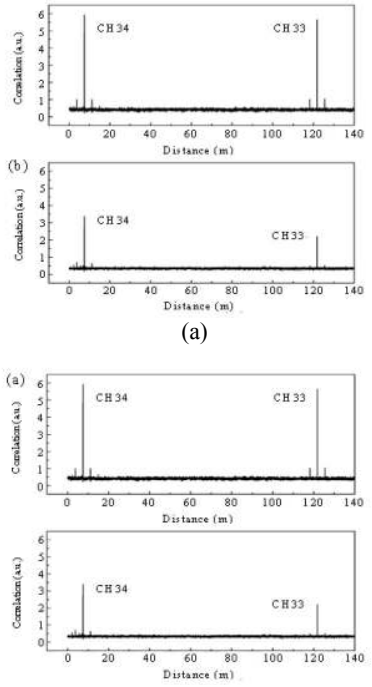

Fig. 30 Correlation spectra of (a) free of strain and (b) strain applied [65].

The dynamic sensing setup is shown in Fig. 31 [65]. The dynamic sensing unit is a section of no-core fiber (NCF) with the length of 29.2 mm, which is spliced to the lead-in SMF and lead-out SMF. NCF is a special fiber which has the same diameter of 125 μm as SMF, but only contains solid cladding and coating made of pure fused silica materials and polymer materials, respectively. The tiny bending of NCF leads to an increase in transmission loss induced by the leaking modes. When NCF vibrates, the light intensity will be modulated by the vibration [101].

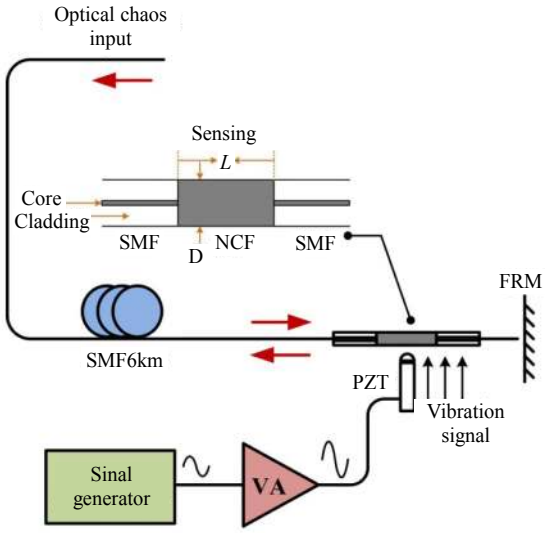

Fig. 31 Schematic of the dynamic strain sensing setup [65].

The locating of sensing point can be accomplished easily from the position of the correlation peaks, similar to that of the static sensing application. For the demodulation of the vibration signal, the reflected signal and the reference signal can be divided into segments in time serial, and the corresponding segments are processed with cross correlation calculation. The correlation peak amplitude of each segment is determined by the reflection light intensity at different recording time slots, which fluctuates with the vibration. Thus, each correlation peak can be seen as a sampling point of vibration. By splicing the correlation curves in time order, we get the fluctuation curve of light intensity from the envelope of correlation peaks, as shown in Fig. 32. Then by conducting the Fourier transformation, the vibration signal can be demodulated [65].

Further, this system possesses a possibility of multi-point sensing along one fiber line. Different points can be distinguished by different positions of correlation peaks. The vibration frequency at each point can be detected by the amplitude variation of the corresponding correlation peak. The wideband chaos also can guarantee the usage of multiple multiplexing methods such as TDM and WDM together in the FOSN and can be extended to many

other sensing parameters, e.g. temperature, refractive index, acceleration, and liquid level, as long as the intensity of chaotic reflection can be modulated by these sensing parameters [65].

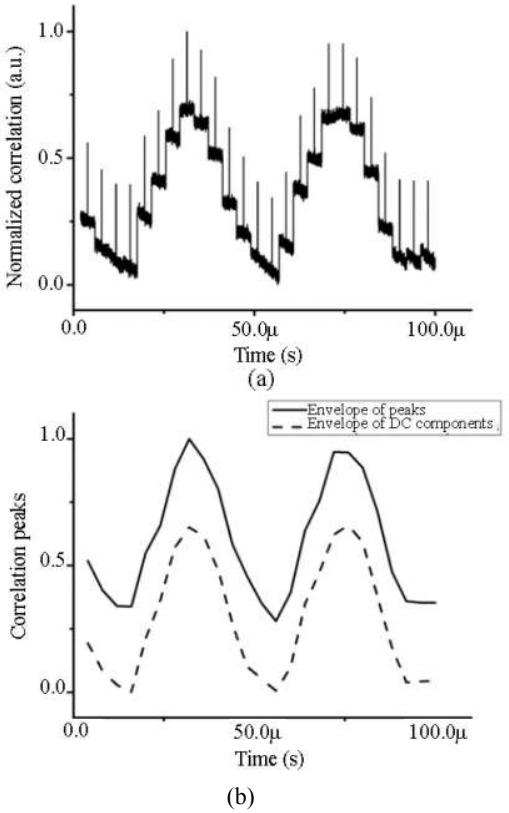

Fig. 32 Vibration demodulation scheme: (a) sampling multiple correlation peak profile and (b) envelope of multiple correlation peaks and direct current (DC) components [65].

8. Conclusions

So far, many efforts to improve the performance of the FOSN have been proposed and realized. Benefiting from the high efficient utilization of the signal resources, the topology architecture of the SPON and hybrid multiplexing based FOSN have shown the advantages of large capacity, flexible access, and integrated management. Further, special fiber lasers as well as the optical chaos have demonstrated the superiorities of high adaptability, good integration, and low cost to meet the requirements of the FOSN. Also, the flexible optical spectrum demodulation technique for sensing signals, as well as the precisely fault monitoring technique for the fiber link have been provided to enhance the sensing performance and survivability of the FOSN. Based on the above key technologies and devices, the FOSN exhibits good adaptiveness for practical application fields such as gas sensing, acoustic sensing, and strain/dynamic strain sensing. The study on the key device and technology of the FOSN will provide the fundamental support and future outlook for fiber sensing.

Acknowledgment

These works are supported by a grant from the Sub-Project of the Major Program of the National Natural Science Foundation of China (No. 61290315), the National Natural Science Foundation of China (No. 61275083, 61275004, and 61404056), the National Key Foundation of Exploring Scientific Instrument of China (No. 2013YQ16048707), and the Fundamental Research Funds for the Central Universities (HUST: No. 2014CG002, and 2014QNRC005). Much appreciation should be given to the students, Zhinlin Xu, Yiyang Luo, Fan Ai , Wei Yang, Enci Chen, Shun Wang ,Shui Zhao, Li Liu, Hao Liao, Xin Fu, Shun Wang, Wei Yang, Wang Yang, and Mingren Su.

References

[1] S. Huang, W. Lin, and M. Chen, "Time-division multiplexing of polarization-insensitive fiber-optic Michelson interferometric sensors," *Optics Letters*, 1995, 20(11): 1244–1246.

[2] D. T. Jenstrom and C. L. Chen, "A fiber optic microbend tactile sensor array," *Sensors and Actuators*, 1989, 20(3): 239–248.

[3] G. Stewart, C. Tandy, D. Moodie, M. A. Morante, and F. Dong, "Design of a fibre optic multi-point sensor

for gas detection," *Sensors and Actuators B: Chemical*, 1998, 51(98): 227–232.

[4] C. Zhou, Y. Rao, and J. Jiang, "A coarse wavelength-division-multiplexed extrinsic fiber Fabry-Perot sensor system," in *Proc. SPIE*, vol. 5634, pp. 219–224, 2005.

[5] Z. Wang, F. Shen, L. Song, X. Wang, and A. Wang, "Multiplexed fiber Fabry-Perot interferometer sensors based on ultrashort Bragg gratings," *IEEE Photonics Technology Letters*, 2007, 19(8): 622–624.

[6] B. J. Vakoc, M. J. F. Digonnet, and G. S. Kino, "A novel fiber-optic sensor array based on the Sagnac interferometer," *Journal of Lightwave Technology*, 1999, 17(11): 2316–2326.

[7] H. Fu, D. Chen, and Z. Cai, "Fiber sensor systems based on fiber laser and microwave photonic technologies," *Sensors*, 2012, 12(5): 5395–5419.

[8] R. A. Perez-Herrera, M. Fernandez-Vallejo, and M. Lopez-Amo, "Robust fiber-optic sensor networks," *Photonic Sensors*, 2012, 2(4): 366–380.

[9] G. R. Kirikera, O. Balogun, and S. Krishnaswamy, "Adaptive fiber Bragg grating sensor network for structural health monitoring: applications to impact monitoring," *Structure Health Monitoring*, 2011, 10(1): 5–16.

[10] C. Chan, W. Jin, H. L. Ho, and M. Suleyman Demokan, "Performance analysis of a time-division-multiplexed fiber Bragg grating sensor array by use of a tunable laser source," *IEEE Journal of Selected Topics in Quantum Electronics*, 2000, 6(5): 741–749.

[11] D. Cooper, T. Coroy, and P. Smith, "Time-division multiplexing of large serial fiber-optic Bragg grating sensor arrays," *Applied Optics*, 2001, 40(16): 2643–2654.

[12] Y. Dai, Y. Liu, J. Leng, G. Deng, and A. Asundi, "A novel time-division multiplexing fiber Bragg grating sensor interrogator for structural health monitoring," *Optics and Lasers in Engineering*, 2009, 47(10): 1028–1033.

[13] M. Zhang, Q. Sun, Z. Wang, X. Li, H. Liu, and D. M. Liu, "A large capacity sensing network with identical weak fiber Bragg gratings multiplexing," *Optics Communications*, 2012, 285(13): 3082–3087.

[14] C. Hu, H. Wen, and W. Bai, "A novel interrogation system for large scale sensing network with identical ultra-weak fiber Bragg gratings," *Journal of Lightwave Technology*, 2014, 32(7): 1406–1411.

[15] G. D. Lloyd, L. Everall, K. Sugden, and I. Bennion, "Resonant cavity time-division-multiplexed fiber Bragg grating sensor interrogator," *IEEE Photonics Technology Letters*, 2004, 16(10): 2323–2325.

[16] Y. Yu, L. Lui, H. Y. Tam, and W. Chung, "Fiber-laser based wavelength division multiplexed fiber Bragg grating sensor system," *IEEE Photonics Technology Letters*, 2001, 13(7): 702–704.

[17] K. Takada, "High-resolution OFDR with incorporated fiber-optic frequency encoder," *IEEE Photonics Technology Letters*, 1992, 4(9): 1069–1072.

[18] B. A. Childers, M. E. Froggatt, S. G. Allison, T. C. Moore, D. A. Hare, C. F. Batten, *et al*., "Use of 3000 Bragg grating strain sensors distributed on four 8-m optical fibers during static load tests of a composite structure," in *Proc. SPIE*, vol. 4332, pp. 133–142, 2001.

[19] J. L. Brooks, R. H. Wentworth, R. C. Youngquist, M. Tur, Y. K. Byoung, and H. J. Shaw, "Coherence multiplexing of fiber-optic interferometric sensors," *Journal of Lightwave Technology*, 1985, 3(5): 1062–1072.

[20] Y. Rao, K. Kalli, G. Brady, D, J, Webb, D. A. Jackson, L. Zhang, *et al*., "Spatially-multiplexed fibre-optic Bragg grating strain and temperature sensor system based on interferometric wavelength-shift detection," *Electronics Letters*, 1995, 31(12): 1009–1010.

[21] Y. Rao, D. A. Jackson, L. Zhang, and I. Bennion, "Strain sensing of modern composite materials with a spatial/wavelength-division multiplexed fiber grating network," *Optics Letters*, 1996, 21(9): 683–685.

[22] Y. Rao, A. B. L. Ribeiro, D. A. Jackson, L. Zhang, and I. Bennion, "Simultaneous spatial, time and wavelength division multiplexed in-fibre grating sensing network," *Optics Communications*, 1996, 125(1): 53–58.

[23] Q. Sun, X. Li, M. Zhang, Q. Liu, H. Liu, and D. Liu, "High capacity fiber optic sensor networks using hybrid multiplexing techniques and their applications," in *Proc. SPIE*, vol. 9044, pp. 90440L-1–90440L-10, 2013.

[24] X. Li, Q. Sun, J. Wo, M. Zhang, and D. Liu, "Hybrid TDM/WDM based fiber-optic sensor network for perimeter intrusion detection," *Journal of Lightwave Technology*, 2012, 30(8): 1113–1120.

[25] X. Li, Q. Sun, D. Liu, R. Liang, J. Zhang, J. Wo, *et al.*, "Simultaneous wavelength and frequency encoded microstructure based quasi-distributed temperature sensor," *Optics Express*, 2012, 20(11): 12076–12084.

[26] Z. Zhang, L. Zhan, K. Xu, J. Wu, Y. Xia, and J. Lin,

"Multiwavelength fiber laser with fine adjustment, based on nonlinear polarization rotation and birefringence fiber filter," *Optics Letters*, 2008, 33(4): 324–326.

[27] Y. Song, L. Zhan, S. Hu, Q. Ye, and Y. Xia, "Tunable multiwavelengthBrillouin-erbium fiber laser with a polarization-maintaining fiber sagnac loop filter," *IEEE Photonics Technology Letters*, 2004, 16(9): 2015–2017.

[28] H. Dong, G. Zhu, Q. Wang, H. Sun, N. K. Dutta, J. Jaques, *et al*., "Multiwavelength fiber ring laser source based on a delayed interferometer," *IEEE Photonics Technology Letters*, 2005, 17(2): 303–305.

[29] Y. Han, X. Dong, C. Kim, M. Jeong, and J. Lee, "Flexible all fiber Fabry-Pérot filters based on superimposed chirped fiber Bragg gratings with continuous FSR tunability and its application to a multiwavelength fiber laser," *Optics Express*, 2007, 15(6): 2921–2926.

[30] Y. G. Han, C. S. Kim, J. U. Kang, and U. C. Peak, "Multiwavelength Raman fiber-ring laser based on tunable cascaded long-period fiber gratings," *IEEE Photonics Technology Letters*, 2003, 15(3): 383–385.

[31] J. Yang, S. C. Tjin, and N. Q. Ngo, "Multiwavelength tunable fiber ring laser based on sampled chirp fiber Bragg grating," *IEEE Photonics Technology Letters*, 2014, 16(4): 1026–1028.

[32] X. Jiang, Q. Yang, G. Vienne, Y. Li, L. Tong, J. Zhang, *et al*., "Demonstration of microfiber knot laser," *Applied Physics Lett*ers, 2006, 89(14): 143513.

[33] W. Fan, J. Gan, Z. Zhang, X. Wei, S. Xu, and Z. Yang, "Narrow linewidth single frequency microfiber laser," *Optics Letters*, 2012, 37(20): 4323–4325.

[34] A. Sulaiman, S. W. Harun, H. Arof, and H. Ahmad, "Compact and tunable erbium-doped fiber laser with microfiber Mach-Zehnder interferometer," *IEEE Journal of Quantum Electronics*, 2012, 48(9): 1165–1168.

[35] W. Jia, Q. Sun, X. Sun, J. Wo, Z. Xu, D. Liu, *et al*., "Wideband microfiber Fabry-Perot filter and its application to multiwavelength fiber ring laser," *IEEE Photonics Technology Letters*, 2014, 26(10), 961–964.

[36] W. Jia, Q. Sun, Z. Xu, X. Sun, and D. Liu, "Channel-spacing tunable multiwavelength erbium-doped fiber laser based on a microfiber Fabry-Perot filter," in *2014 Conference on Lasers and Electro-Optics*, San Jose, pp. 1–2, 2014.

[37] J. Geng and S. Jiang, "Fiber lasers: the 2μm market heats up," *Optics and Photonics News*, 2014, 25(7): 4–41.

[38] F. McALeavey, B. D. MacCraith, J. O'Gorman, and J. Hegarty, "Tunable and efficient diode-pumped Tm^{3+}-doped fluoride fiber laser for hydrocarbon gas sensing," *Fiber & Integrated Optics*, 1997, 16(4): 355–368.

[39] Q. Mao and J. W. Y. Lit, "Switchable multiwavelength erbium-doped fiber laser with cascaded fiber grating cavities," *IEEE Photonics Technology Letters*, 2002, 14(5): 612–614.

[40] S. Liu, F. Yan, T. Feng, B. Wu, Z. Dong,k and G. K. Chang, "Switchable and spacing-tunable dual-wavelength thulium-doped silica fiber laser based on a nonlinear amplifier loop mirror," *Applied Optics*, 2014, 53(24): 5522–5526.

[41] X. Ma, S. Luo, and D. Chen, "Switchable and tunable thulium-doped fiber laser incorporating a Sagnac loop mirror," *Applied Optics*, 2014, 53(20): 4382–4385.

[42] S. Liu, F. Yan, W. Peng, T. Feng Z. Dong, and G. Chang, "Tunable dual-wavelength thulium-doped fiber laser by employing a HB-FBG," *IEEE Photonics Technology Letters*, 2014, 26(18): 1809–1812.

[43] W. Peng, F. Yan, Q. Li, S. Liu, T. Feng, S. Y. Tan, *et al*., "1.94 μm switchable dual-wavelength Tm^{3+} fiber laser employing high-birefringence fiber Bragg grating," *Applied Optics*, 2013, 52(19): 4601–4607.

[44] M. Delgado-Pinar, J. Mora, A. Díez, J. L. Cruz, and M. V. Andrés, "Wavelength-switchable fiber laser using acoustic waves," *IEEE Photonics Technology Letters*, 2005, 17(3): 552–554.

[45] S. Zhao, P. Lu, D. Liu, and J. Zhang, "Switchable multiwavelength thulium-doped fiber ring lasers," *Optical Engineering*, 2013, 52(8): 086105–086111.

[46] W. Yang, P. Lu, S. Wang, D. Liu, and J. Zhang, "2-μm switchable, tunable and power-controllable dual-wavelength fiber laser based on parallel cavities using 3×3 coupler," *Applied Physics B*, 2015, 120(2): 349–354.

[47] M. A. Putnam, M. L. Dennis, I. N. Duling, C. G. Askins, and E. J. Friebele, "Broadband square-pulse operation of a passively mode-locked fiber laser for fiber Bragg grating interrogation," *Optics Letters*. 1998, 23(2): 138–140.

[48] M. A. Solodyankin, E. D. Obraztsova, A. S. Lobach, A. I. Chernov, A. V. Tausenev, V. I. Konov, *et al*.,

"Mode-locked 1.93 mm thulium fiber laser with a carbon nanotube absorber," *Optics Letters*, 2008, 33(12): 1336–1338.

[49] F. Bonaccorso, Z. Sun, T. Hasan, and A. C. Ferrari, "Graphene photonics and optoelectronics," *Nature Photonics*, 2010, 4(9): 611–622.

[50] X. Liu, "Interaction and motion of solitons in passively-mode-locked fiber lasers," *Physical Review A*, 2011, 84(5): 1688–1690.

[51] Z. Sun, T. Hasan, F. Wang, A. G. Rozhin, I. H. White, and A. C. Ferrari, "Ultrafast stretched-pulse fiber laser mode-locked by carbon nanotubes," *Nano Research*, 2010, 3(6): 404–411.

[52] K. Kieu and F. W. Wise, "All-fiber normal-dispersion femtosecond laser," *Optics Express*, 2008, 16(15): 11453–11458.

[53] L. R. Chen, G. E. Town, P. Y. Cortès, S. LaRochelle, and P. W. E. Smith, "Dual-wavelength, actively mode-locked fibre laser with 0.7 nm wavelength spacing," *Electronics Letters*, 2000, 36(23): 1921–1923.

[54] S. Pan and C. Lou, "Stable multiwavelength dispersion-tuned actively mode-locked erbium-doped fiber ring laser using nonlinear polarization rotation," *IEEE Photonics Technology Letters*, 2006, 18(13): 1451–1453.

[55] D. Pudo and L. R. Chen, "Actively mode locked, quadruple-wavelength fibre laser with pump-controlled wavelength switching," *Electronics Letters*, 2003, 39(3): 272–274.

[56] Z. Yan, X. Li, Y. Tang, P. P. Shum, X. Yu, Y. Zhang, *et al*., "Tunable and switchable dual-wavelength Tm-doped modelocked fiber laser by nonlinear polarization evolution," *Optics Express*, 2015, 23(4): 4369–4376.

[57] J. Sotor, G. Sobon, I. Pasternak, A. Krajewska, W. Strupinski, and K. M. Abramski, "Simultaneous mode-locking at 1565 and 1944 nm in fiber laser based on common graphene saturable absorber," *Optics Express*, 2013, 21(16): 18994–19002.

[58] Y. Luo, Q. Sun, Z. Wu, Z. Xu, S. Fu, L. Zhao, *et al*., "258-MHz group velocity locked vector dissipative solitons in a dispersion-managed short-cavity fiber laser," in *Optoelectronic Global Conference*, China, pp. 29–31, 2015.

[59] Y. Wang, B. Wang, and A. Wang, "Chaotic correlation optical time domain reflectometer utilizing laser diode," *IEEE Photonics Technology Letters*, 2008, 20(19): 1636–1638.

[60] A. Wang, N. Wang, Y. Yang, B. Wang, M. Zhang, and Y. Wang, "Precise fault location in WDM-PON by utilizing wavelength tunable chaotic laser," *Journal of Lightwave Technology*, 2012, 30(21): 3420–3426.

[61] L. Xia, D. Huang, J. Xu, and D. Liu, "Simultaneous and precise fault locating in WDM-PON by the generation of optical wideband chaos," *Optics Letters*, 2013, 38(19): 3762–3764.

[62] C. Jáuregui, J. M. López-Higuera, A. Cobo, O. M. Conde, and J. Zubía, "Multiparameter sensor based on a chaotic fiber-ring resonator," *Journal of the Optical Society of America B*, 2006, 23(10): 2024–2031.

[63] X. Zhang and L. Yang, "A fiber Bragg grating quasi-distributed sensing network with a wavelength-tunable chaotic fiber laser," *Systems Science and Control Engineering*, 2014, 2(1): 268–274.

[64] Z. Ma, M. Zhang, Y. Liu, X. Bao, H. Liu, Y. Zhang, *et al*., "Incoherent Brillouin optical time-domain reflectometry with random state correlated Brillouin spectrum," *IEEE Photonics Journal*, 2015, 7(4): 1–7.

[65] L. Xia, C. Yu, Y. Ran, J. Xu, and W. Li, "Static/dynamic strain sensing applications by monitoring the correlation peak from optical wideband chaos," *Optics Express*, 2015, 23(20): 26113–26123.

[66] Y. Luo, L. Xia, Z. Xu, C. Yu, Q. Sun, W. Li, *et al*., "Optical chaos and hybrid WDM/TDM based large capacity quasi-distributed sensing network with real-time fiber fault monitoring," *Optics Express*, 2015, 23(3): 2416–2423.

[67] C. G. Askins, M. A. Putnam, and E. J. Friebele, "Instrumentation for interrogating many-element fiber Bragg grating arrays," in *Proc. SPIE*, vol. 2444, pp. 257–266, 1995.

[68] A. D. Kersey, M. A. Davis, and H. J. Patrick, "Fiber grating sensors," *Journal of Lightwave Technology*, 1997, 15(8): 1442–1463.

[69] A. D. Kersey, T. A. Berkoff, and W. W. Morey, "Multiplexed fiber Bragg grating strain-sensor system with a fiber Fabry-Perot wavelength filter," *Optics Letters*, 1993, 18(16): 1370–1372.

[70] G. Yang, J. H. Guo, G. L. Xu, L. D. Lv, G. J. Tu, and L. Xia, "A novel fiber Bragg grating wavelength demodulation system based on F-P etalon," in *Proc. SPIE*, vol. 9270, pp. 92700V-1–92700V-7, 2014.

[71] D. M. Baney, B. Szafraniec, and A. Motamedi, "Coherent optical spectrum analyzer," *IEEE Photonics Technology Letters*, 2002, 14(3): 355–357.

[72] Q. Sun, J. Cheng, F. Ai, X. Li, D. Liu, and L. Zhang, "High speed and high resolution demodulation system for hybrid WDM/FDM based fiber microstructure sensor network by using Fabry-Perot filter," in *2015 Conference on Lasers and Electro-Optics*, San Jose, pp. 1–2, 2015.

[73] F. Ai, Q. Sun, J. Cheng, and D. Liu, "High resolution demodulation platform for large capacity hybrid WDM/FDM microstructures sensing system assisted by tunable FP filter," in *Progress in Electromagnetics Research Symposium*, Cambridge, pp. 1200–1203, 2015.

[74] M. Legre, R. Thew, and H. Zbinden, "High resolution Optical Time Domain Reflectometer based on 1.55 μm up-conversion photon-counting module," *Optics Express*, 2007, 15(13): 8237–8242.

[75] J. H. Park, J. S. Baik, and C. H. Lee, "Fault-detection technique in a WDM-PON," *Optics Express,* 2007, 15(4): 1461–1466.

[76] Y. Luo, L. Xia, Z. Xu, C. Yu, Q. Sun, W. Li, *et al*., "Optical chaos and hybrid WDM/TDM based large capacity quasi-distributed sensing network with real-time fiber fault monitoring," *Optics Express*, 2015, 23(3): 2416–2423.

[77] J. Hodgkinson and R. P. Tatam, "Optical gas sensing: a review," *Measurement Science & Technology*, 2012, 24(1): 111–123.

[78] H. Waechter, J. Litman, A. H. Cheung, J. A. Barnes, and H. P. Loock, "Chemical sensing using fiber cavity ring-down spectroscopy," *Sensors*, 2010, 10(3): 1716–1742.

[79] X. Sun, Q. Sun, S. Zhu, Y. Yuan, Z. Huang, X. Liu, *et al*., "High sensitive ammonia gas sensor based on graphene coated microfiber," in *PIERS Proceedings*, Prague, pp. 1196–1199, 2015.

[80] Z. Gu, Y. Xu, and K. Gao, "Optical fiber long-period grating with solgel coating for gas sensor," *Optics Letters*, 2006, 31(16): 2405–2407, 2006.

[81] W. Jin, H. Ho, Y. Cao, J. Ju, and L. Qi, "Gas detection with micro- and nano-engineered optical fibers," *Optical Fiber Technology*, 2013, 19(6): 741–759.

[82] J. Henningsen and J. Hald, "Dynamics of gas flow in hollow core photonic bandgap fibers," *Applied Optics*, 2008, 47(15): 2790–2797.

[83] J. P. Parry, B. C. Griffiths, N. Gayraud, E. D. McNaghten, A. M. Parkes, W. N. MacPherson, *et al*., "Towards practical gas sensing with micro-structured fiber," *Measurement Science and Technology*, 2009, 20(7): 190–190.

[84] G. Stewart, C. Tandy, D. Moodie, M. A. Morante, and F. Dong, "Design of a fiber optic multi-point sensor for gas detection," *Sensors and Actuators B: Chemical*, 1998, 51(1): 227–232.

[85] W. Jin, "Performance analysis of a time-division-multiplexed fiber-optic gas-sensor array by wavelength modulation of a distributed-feedback laser," *Applied optics*, 1999, 38(25): 5290–5297.

[86] G. Whitenett, G. Stewart, H. B. Yu, and B. Culshaw, "Investigation of a tuneable mode-locked fiber laser for application to multipoint gas spectroscopy," *Journal of Lightwave Technology*, 2004, 22(3): 813–819.

[87] M. Završnik and G. Stewart, "Theoretical analysis of a quasi-distributed optical sensor system using FMCW for application to trace gas measurement," *Sensors and Actuators B: Chemical*, 2000, 71(1): 31–35.

[88] F. Ye, L. Qian, and B. Qi, "Multipoint chemical gas sensing system based on frequency-shifted interferometry," *Conference on Optical Fiber Communication/National Fiber Optic Engineers Conference, 2008*, San Diego, United States, pp. 1–3, 2008.

[89] W. Zhang, Y. Lu, L. Duan, Z. Zhao, W. Shi, and J. Yao, "Intracavity absorption multiplexed sensor network based on dense wavelength division multiplexing filter," *Optics Express*, 2014, 22(20): 24545–24550.

[90] OptoSniff/Optosci, http://www.optosniff.com/.

[91] C. Caliendo, "Latest trends in acoustic sensing," *Sensors*, 2014, 14(4): 5781–5784.

[92] C. K. Kirkendall and A. Dandridge, "Overview of high performance fibre-optic sensing," *Journal of Physics D: Applied Physics*, 2004, 37(18): R197–R216.

[93] J. G. Teixeira, I. T. Leite, S. Silva, and O. Frazão, "Advanced fiber-optic acoustic sensors," *Photonic Sensors*, 2014, 4(3): 198–208.

[94] S. Foster, A. Tikhomirov, M. Milnes, J. van Velzen, and G. Hardy, "A fiber laser hydrophone," in *Proc. SPIE*, vol. 5855, pp. 627–630, 2005.

[95] R. Chen, G. F. Fernando, T. Butler, and R. A. Badcock, "A novel ultrasound fibre optic sensor based on a fused-tapered optical fibre coupler," *Measurement Science and Technology*, 2004, 15(8): 1490–1495.

[96] B. Xu, Y. Li, M. Sun, Z. Zhang, X. Dong, Z. Zhang, *et al*., "Acoustic vibration sensor based on

nonadiabatic tapered fibers," *Optics Letters*, 2012, 37(22): 4768–4770.

[97] J. P. Mutschlecner and R. W. Whitaker, "Infrasound from earthquakes," *Journal of Geophysical Research: Atmospheres*, 2005, 110(110): 372–384.

[98] S. Wang, P. Lu, L. Zhang, D. Liu, and J. Zhang, "Optical fiber acoustic sensor based on nonstandard fused coupler and aluminum foil," *IEEE Sensors Journal*, 2014, 14(7): 2293–2298.

[99] S. Wang, P. Lu, L. Zhang, D. Liu, and J. Zhang, "Intensity demodulation-based acoustic sensor using dual fiber Bragg gratings and a titanium film," *Journal of Modern Optics*, 2014, 61(12): 1033–1038.

[100] S. Wang, P. Lu, H. Liao, L. Zhang, D. Liu, and J. Zhang, "Passively mode-locked fiber laser sensor for acoustic pressure sensing," *Journal of Modern Optics*, 2013, 60(21): 1892–1897.

[101] Y. Ran, L. Xia, Y. Han, W. Li, J. Rohollahnejad, Y. Wen, *et al*., "Vibration fiber sensors based on SM-NC-SM fiber structure," *IEEE Photonics Journal*, 2015, 7(2): 1–7.